BIOCHEMISTRY
including biophysical chemistry & molecular biology

Article

Kinetic and Thermodynamic Characterization of the RNA Guanylyltransferase Reaction

Marie F. Soulière, Jean-Pierre Perreault, and Martin Bisaillon

Biochemistry, **2008**, 47 (12), 3863-3874 • DOI: 10.1021/bi702054a • Publication Date (Web): 26 February 2008

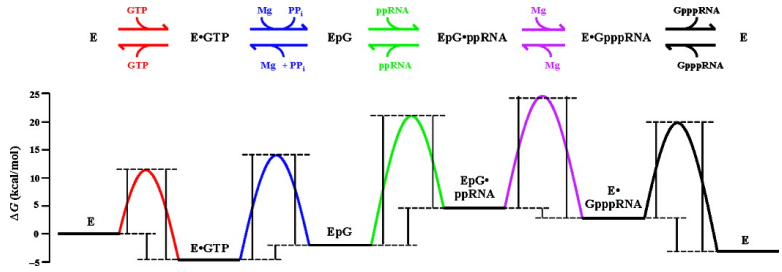

More About This Article

Additional resources and features associated with this article are available within the HTML version:

- Supporting Information
- Access to high resolution figures
- Links to articles and content related to this article
- Copyright permission to reproduce figures and/or text from this article

View the Full Text HTML

Kinetic and Thermodynamic Characterization of the RNA Guanylyltransferase Reaction†

Marie F. Soulière, Jean-Pierre Perreault, and Martin Bisaillon*

RNA Group/Grpe ARN, Département de Biochimie, Faculté de Médecine et des Sciences de la Santé, Université de Sherbrooke, Sherbrooke, Quebec J1H 5N4, Canada

Received October 12, 2007; Revised Manuscript Received December 13, 2007

ABSTRACT: An RNA guanylyltransferase activity is involved in the synthesis of the cap structure found at the 5′ end of eukaryotic mRNAs. The RNA guanylyltransferase activity is a two-step ping-pong reaction in which the enzyme first reacts with GTP to produce the enzyme−GMP covalent intermediate with the concomitant release of pyrophosphate. In the second step of the reaction, the GMP moiety is then transferred to a diphosphorylated RNA. Both reactions were previously shown to be reversible. In this study, we report a biochemical and thermodynamic characterization of both steps of the reaction of the RNA guanylyltransferase from *Paramecium bursaria Chlorella* virus 1, the prototype of a family of viruses infecting green algae. Using a combination of real-time fluorescence spectroscopy, radioactive kinetic assays, and inhibition assays, the complete kinetic parameters of the RNA guanylyltransferase were determined. We produced a thermodynamic scheme for the progress of the reaction as a function of the energies involved in each step. We were able to demonstrate that the second step comprises the limiting steps for both the direct and reverse overall reactions. In both cases, the binding to the RNA substrates is the step requiring the highest energy and generating unstable intermediates that will promote the catalytic activites of the enzyme. This study reports the first thorough kinetic and thermodynamic characterization of the reaction catalyzed by an RNA capping enzyme.

The 5′ ends of most eukaryotic mRNAs and many viral mRNAs harbor a ^{m7}GpppN cap structure that plays a critical role in the translation and stability of mRNAs (*1*). Synthesis of this cap structure involves three distinct enzymatic activities (*2*). (a) The 5′ end of pre-mRNAs is initially hydrolyzed to a diphosphate end by an RNA triphosphatase. (b) The diphosphate end of the mRNA is then capped with GMP by an RNA guanylyltransferase, and finally, (c) the cap is methylated by an RNA (guanine-7) methyltransferase.

$$\text{pppGpN}- \rightarrow \text{ppGpN}- + \text{P}_\text{i} \quad \text{(a)}$$

$$\text{ppGpN}- + \text{pppG} \rightleftarrows \text{GpppGpN}- + \text{PP}_\text{i} \quad \text{(b)}$$

$$\text{GpppGpN}- + \text{Ado-Met} \rightarrow {}^{m7}\text{GpppGpN-G} + \text{Ado-Hcy} \quad \text{(c)}$$

The RNA guanylyltransferase activity is a two-step ping-pong reaction (*1, 2*) in which the enzyme first reacts with GTP to produce the enzyme−GMP (EpG) covalent intermediate with the concomitant release of pyrophosphate (i). In the second step of the reaction, the GMP moiety is then transferred to a diphosphorylated RNA (ii).

$$\text{E} + \text{ppp}^{\alpha}\text{G} \rightleftarrows \text{Ep}^{\alpha}\text{G} + \text{PP}_\text{i} \quad \text{(i)}$$

$$\text{Ep}^{\alpha}\text{G} + \text{ppGpN}- \rightleftarrows \text{G}^{\alpha}\text{pppGpN}- + \text{E} \quad \text{(ii)}$$

Both reactions were previously shown to be reversible and to require divalent cations to occur (*3*).

Eukaryotic viruses have developed many strategies to ensure the translation of their mRNAs. A number of viruses which replicate in the cytoplasm of the infected cells encode enzymes involved in RNA cap synthesis enzymes (*4*). Other viruses like adenoviruses and influenza virus are known to use the enzymes of the host cells to synthesize their cap structure and to steal the cap from cellular mRNAs to cap their own viral mRNAs, respectively (*5, 6*). *Paramecium bursaria Chlorella* virus 1 (PBCV-1) is a large icosahedral virus, the prototype of a family of viruses infecting green algae, which encodes more then 375 different proteins, including two enzymes involved in the synthesis of the cap structure of mRNAs (*7*). The A449R gene encodes an RNA 5′-triphosphatase (*8*), whereas the A103R gene is translated into a single polypeptide of 330 amino acids which displays RNA guanylyltransferase activity (*9*). This protein is the smallest enzyme harboring this activity involved in the synthesis of the cap structure of mRNAs (*9, 10*). The identity of the viral or cellular protein involved in the methylation of the capping guanosine found at the 5′ ends of the PBCV-1 mRNAs remains unknown.

The PBCV-1 RNA guanylyltransferase is a member of the RNA/DNA nucleotidyltransferase superfamily (*11, 12*) which includes both DNA and RNA ligases. The members of this family contain a conserved active site motif (KxDG) in which the lysine residue is involved in the formation of

† This work was supported by a grant from the Canadian Institutes for Health Research. M.B. is a New Investigator Scholar from the Canadian Institutes for Health Research. J.-P.P. holds the Canada Research Chair in Genomics and Catalytic RNA.

* To whom correspondence should be addressed. Phone: (819) 564-5227. Fax: (819) 564-5340. E-mail: Martin.Bisaillon@USherbrooke.ca.

10.1021/bi702054a CCC: $40.75
Published on Web 02/26/2008

the enzyme−GMP (capping) or enzyme−AMP (ligases) intermediates (*11*). Elucidation of the crystal structure of the PBCV-1 A103R protein has provided insightful information about the RNA guanylyltransferase reaction (*10, 13*). Examination of the crystals suggested that a large conformational change occurs upon GTP binding, shifting the structure from an open to a closed conformation (*10, 13*). A model in which the conformational change encountered upon GTP binding would promote metal ion binding and guanylylation has been suggested (*10, 13*).

We report here a biochemical characterization of both steps of the RNA guanylyltransferase. In an effort to gain further knowledge of the RNA guanylyltransferase reaction, fluorescence spectroscopy, radioactive kinetics, and filter binding assays were performed in evaluating the kinetic parameters involved in both steps of the catalytic reaction. This study provides a detailed picture of the energetics involved in the reaction chemistry. Such analyses are crucial for allowing an improved understanding of the thermodynamic basis of the RNA guanylyltransferase reaction.

MATERIALS AND METHODS

Expression and Purification of Recombinant A103R Protein. A plasmid for the expression of a full-length A103R protein (330 amino acids) was generated by inserting the *Chlorella* virus A103R gene between the *Nhe*I and *Hin*dIII cloning sites of the pET28a expression plasmid (Novagen). In this context, the A103R protein is fused in frame with an N-terminal peptide containing six tandem histidine residues, and expression of the His-tagged protein is driven by a T7 RNA polymerase promoter. The resulting recombinant plasmid (pET-A103R) was transformed into *Escherichia coli* BL21(DE3), and a 1 L culture of *E. coli* BL21(DE3)/pET-A103R was grown at 37 °C in Luria-Bertani medium containing 0.1 mg/mL ampicillin until the A_{600} reached 0.5. The culture was adjusted to 0.4 mM isopropyl β-D-thiogalactopyranoside and 2% ethanol, and the incubation continued at 18 °C for 20 h. The cells were then harvested by centrifugation at 5000 rpm for 15 min, and the pellets were stored at −80 °C. All subsequent procedures were performed at 4 °C. Thawed pellets of bacteria were resuspended in 50 mL of lysis buffer A [50 mM Tris-HCl (pH 7.5), 150 mM NaCl, and 10% sucrose], and cell lysis was achieved by adding lysozyme and Triton X-100 to final concentrations of 50 μg/mL and 0.1%, respectively. The lysates were sonicated to reduce viscosity, and any insoluble material was removed by centrifugation at 13000 rpm for 45 min. The soluble extract was applied to a 2 mL column of nickel−nitrilotriacetic acid−agarose (Qiagen) that had been equilibrated with buffer A containing 0.1% Triton X-100. The column was washed with the latter buffer and then eluted stepwise with buffer B [50 mM Tris-HCl (pH 8.0), 100 mM NaCl, and 10% glycerol] containing 50, 100, 200, 500, and 1000 mM imidazole. The polypeptide composition of the column fractions was monitored by SDS−PAGE. The recombinant A103R protein was retained on the column and recovered in the 500 and 1000 mM imidazole eluates. Following a 2 h dialysis against buffer C [50 mM Tris-HCl (pH 8.0), 50 mM NaCl, 2 mM dithiothreitol, and 10% glycerol] with 5 mM potassium pyrophosphate, a second 2 h dialysis was performed against buffer C alone. The protein concentration in the recovered fraction was determined by the Bio-Rad dye binding method using bovine serum albumin as the standard, and the proteins were stored at −80 °C.

Purification of the EpG Complex. The purified A103R protein was allowed to react with [α-^{32}P]GTP in the presence of 5 mM $MgCl_2$, 50 mM Tris-HCl (pH 8.0), 5 mM DTT, and 1.25 μg/mL inorganic yeast pyrophosphatase (Roche), to produce the covalent intermediate Ep[α-^{32}]G. The covalent intermediate was applied to a 2 mL column of nickel−nitrilotriacetic acid−agarose (Qiagen) that had been equilibrated with buffer A containing 0.1% Triton X-100. The column was washed with the latter buffer and then eluted stepwise with buffer B [50 mM Tris-HCl (pH 8.0), 100 mM NaCl, and 10% glycerol] containing 50, 100, 200, 500, and 1000 mM imidazole. The polypeptide composition of the column fractions was monitored by SDS−PAGE. The radiolabeled EpG intermediate was retained on the column and recovered in the 500 and 1000 mM imidazole eluates, while the remaining [α-^{32}P]GTP, ions, and pyrophosphatase were eluted in lower fractions. The presence of the radiolabeled intermediate was revealed by autoradiography with a PhosphorImager (Amersham Biosciences). The extent of protein guanylation was observed by Coomassie staining, and an efficiency of 100% was commonly observed.

Radioactive Pyrophosphate Synthesis. Reaction mixtures containing 50 mM Tris-HCl (pH 8.0), 5 mM DTT, 5 mM $MgCl_2$, 10 μL of [γ-^{32}P]GTP, and 10 μM A103R protein were incubated at 30 °C for 10 min. Unlabeled GTP (500 μM) was then added to the mixture, and further incubation was carried out at 30 °C for 15 min. The reaction was stopped with 20 mM formic acid and then the mixture spotted on a thin layer chromatography (TLC) sheet with controls of GTP and pyrophosphate. The TLC was migrated for 1 h in a migration buffer (1 M formic acid and 1.5 M LiCl). The pyrophosphate migration was then observed by UV shadowing, the matching layer portion scraped off, and pyrophosphate eluted overnight in 700 μL of 1 M Tris-HCl (pH 7.5). After a 1 min centrifugation at 13000 rpm, the solution containing the radiolabeled pyrophosphate was retrieved and frozen at −20 °C until further use.

Diphosphorylated and Capped RNA Substrate Synthesis. An RNA substrate of 81 nucleotides was synthesized using a PCR template encoding the 5′ terminal portion of the *PBCV*-1 DNA polymerase gene, with a T7 RNA polymerase promoter. For some experiments, the 5′-triphosphorylated RNA transcript was synthesized in the presence of [γ-^{32}P]UTP. Following transcription, the RNA substrate was purified on a denaturing 8% polyacrylamide gel and visualized by ultraviolet shadowing. The corresponding band was excised and then eluted from the gel via an overnight incubation in 0.1% SDS and 0.5 M ammonium acetate. The RNA was then precipitated with 2-propanol, and the pellet was resuspended in nanopure water. The purified 5′-triphosphorylated 81-nucleotide RNA was further processed using the *Chlorella* virus RNA 5′-triphosphatase (*cv*RTP) to obtain a diphosphorylated 5′ end. The diphosphorylated RNA (ppRNA) was purified on an 8% polyacrylamide gel and the corresponding band excised. After precipitation and resuspension, the RNA subtrate was either quantitated by spectrophotometry and stored at −20 °C or allowed to incubate with 100 μM cold or radiolabeled EpG complex for 2 h to produce capped RNA (GpppRNA). This capped

RNA was again purified on a polyacrylamide gel, excised, precipitated, and stored.

Fluorescence Measurements. Fluorescence was measured using a Hitachi F-2500 fluorescence spectrophotometer. Subtracting the signal from either buffer alone or buffer containing the appropriate quantity of substrate eliminated background emission.

The extent of binding of ligand to the A103R protein was determined by monitoring the fluorescence emission of a constant concentration of proteins and titrating with a ligand of interest. Binding can then be described by eq 1:

$$K_D = [\text{A103R}][\text{ligand}][\text{A103R}\cdot\text{ligand}] \quad (1)$$

where K_D is the apparent dissociation constant, [A103R] is the concentration of the protein, [A103R·ligand] is the concentration of the complexed protein, and [ligand] is the concentration of unbound ligand. The measured fluorescence intensity is related to the proportion of ligand-bound protein by eq 2:

$$\Delta F/\Delta F_{max} = [\text{A103R}\cdot\text{ligand}]/[\text{A103R}]_{tot} \quad (2)$$

where ΔF is the observed variation between the fluorescence intensity at a given ligand concentration and the fluorescence intensity in the absence of ligand, ΔF_{max} is the difference at an infinite ligand concentration, and $[\text{A103R}]_{tot}$ is the total protein concentration in solution.

If the total ligand concentration, $[\text{ligand}]_{tot}$, is in large molar excess relative to $[\text{A103R}]_{tot}$, then it can be assumed that [ligand] (unbound ligand) is approximately equal to $[\text{ligand}]_{tot}$. With that assumption, we can combine eqs 1 and 2 to give eq 3:

$$\Delta F/\Delta F_{max} = [\text{ligand}]_{tot}/(K_D + [\text{ligand}]_{tot}) \quad (3)$$

The K_D values were determined from a nonlinear least-squares regression analysis of titration data by using eq 3. Inner filter effects were corrected using the formula

$$F_{corr} = F_{obs} \times \text{antilog}[(A_{ex} + A_{em})/2] \quad (4)$$

where F_{corr} is the corrected fluorescence intensity, F_{obs} is the observed fluorescence intensity, A_{ex} is the absorbance at the excitation wavelength, and A_{em} is the absorbance at the emission wavelength.

First-Step Association Rate Constant Measurements. Real-time GTP binding experiments were performed by fluorescence spectroscopy using a F-2500 fluorescence spectrophotometer. Twenty microliters of GTP solutions (final concentration of 0.01–10 mM) was injected at a predetermined time into 100 μL of 10 μM protein samples in binding buffer [50 mM Tris-HCl (pH 7.5) and 10 mM NaCl]. The samples were excited at 290 nm, and the fluorescence was monitored as a function of time at 332 nm. The results were corrected for the dilution factor by subtracting the relative curves obtained by injection of buffer alone into the samples. The results were analyzed using one-phase exponential association curves.

First-Step Dissociation Rate Constant Measurements. Dissociation reaction mixtures containing 50 mM Tris-HCl (pH 8.0), 5 mM DTT, 0.5 mM EDTA, 1 mM [α-^{32}P]GTP, and 10 μM A103R protein were incubated at 30 °C for 15 min. To dissociate the bound labeled GTP, 5 μL of 500 mM cold GTP was added to 20 μL of reaction mixtures and the reactions were then stopped at various time (0.5–10 s) by adding trichloroacetic acid (TCA) to a final concentration of 12% and 0.75 mg/mL bovine serum albumin (BSA) (*14*). The mixtures in which reactions had been stopped were then allowed to precipitate on ice for 30 min and then centrifuged at 13000 rpm for 15 min. Supernatants were removed, and pellets were washed with ethanol and centrifuged again for 5 min at 13000 rpm. Again, the supernatants were removed, and samples were left to dry at room temperature for 15 min. The amount of remaining bound radioactive GTP was measured using a TriCarb 2200-CA liquid scintillation analyzer. The dissociation data were analyzed using one-phase exponential decay curve analysis.

Inhibition Assays. Reaction mixtures containing 50 mM Tris-HCl (pH 8.0), 5 mM DTT, 5 mM $MgCl_2$, and various [α-^{32}P]GTP concentrations (0.01−10 mM) were incubated in the presence of increasing concentrations of tetrapotassium pyrophosphate (0.05−50 mM) or sodium phosphonoformate tribasic hexahydrate (foscarnet) (0.5−10 mM). The inhibition reactions were stopped by the addition of 50% standard protein loading buffer. The samples were analyzed by migration via 12% SDS−PAGE, and inhibition of the formation of the covalent intermediate was monitored by autoradiography.

Forward Reaction Kinetic Assays. Reaction mixtures containing 50 mM Tris-HCl (pH 8.0), 5 mM DTT, 5 mM $MgCl_2$, and various concentrations of [α-^{32}P]GTP (1−100 μM) or ppRNA (0.01−5 μM) were preincubated at 30 °C for 15 min. Reactions were started by adding 10 μM A103R protein or 100 nM [α-^{32}P]EpG, respectively, and stopped at the predetermined times (10−480 s or 1–40 min, respectively) by 0.15 mM EDTA, 2.5% SDS, and standard protein loading buffer or RNA loading buffer. Samples were then analyzed by migration via 12% SDS−PAGE for 3−4 h or via an 8% polyacrylamide gel for 1 h, and the covalent intermediate (EpG) or GpppRNA formation was detected by autoradiography using a PhosphorImager (Amersham Biosciences). For the first-step forward reaction, 1.5 μg/mL inorganic yeast pyrophosphatase (Roche) was added to the reaction mixtures.

Reverse Reaction Kinetic Assays. Reaction mixtures containing 50 mM Tris-HCl (pH 8.0), 5 mM DTT, 5 mM $MgCl_2$, 30 units of RNA guard (Amersham), and various concentrations of PP_i or A103R protein (1−100 or 0.5−50 μM, respectively) were preincubated at 30 °C for 15 min. The reactions were initiated by adding 1.6 μM radiolabeled EpG complex or 1 μM GpppRNA and stopped at the predetermined times (10−480 s and 1−60 min) by either 150 mM EDTA, 2.5% SDS, and standard protein loading buffer or RNA loading buffer. The samples were then analyzed by migration via 12% SDS−PAGE for 3−4 h or via an 8% polyacrylamide gel for 1 h, and GTP or EpG formation was detected by autoradiography using a PhosphorImager. For the second-step reverse reaction, 1 μg/mL antarctic phosphatase (NEB) was added to the reaction mixtures.

Radioactive Pyrophosphate Binding Assay. Reaction mixtures containing either 50 mM Tris-HCl (pH 7.5), 10 mM NaCl, and 10 μM A103R protein or 50 mM Tris-HCl (pH 7.5), 10 mM NaCl, 10 μM EpG covalent intermediate, 50 mM EDTA, and increasing concentrations of PP_i (from 0.05 to 5.0 mM), containing traces of [β-^{32}P]PP_i, were incubated at 30 °C for 15 min. The reaction mixtures were then precipitated by adding trichloroacetic acid (TCA) to a final

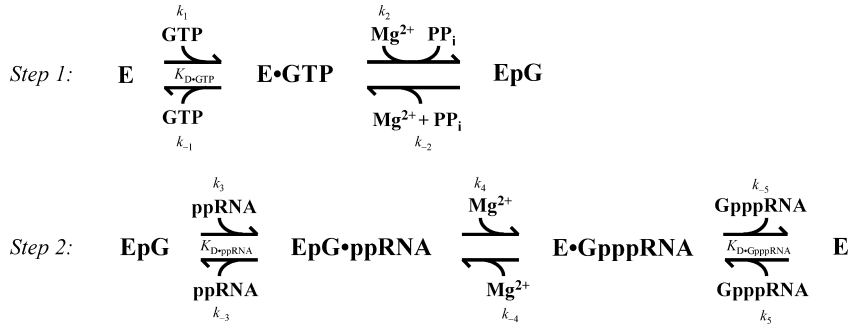

FIGURE 1: RNA guanylyltransferase reaction. An overall view of each step of the RNA guanylyltransferase reaction. The kinetic constants to be determined are indicated.

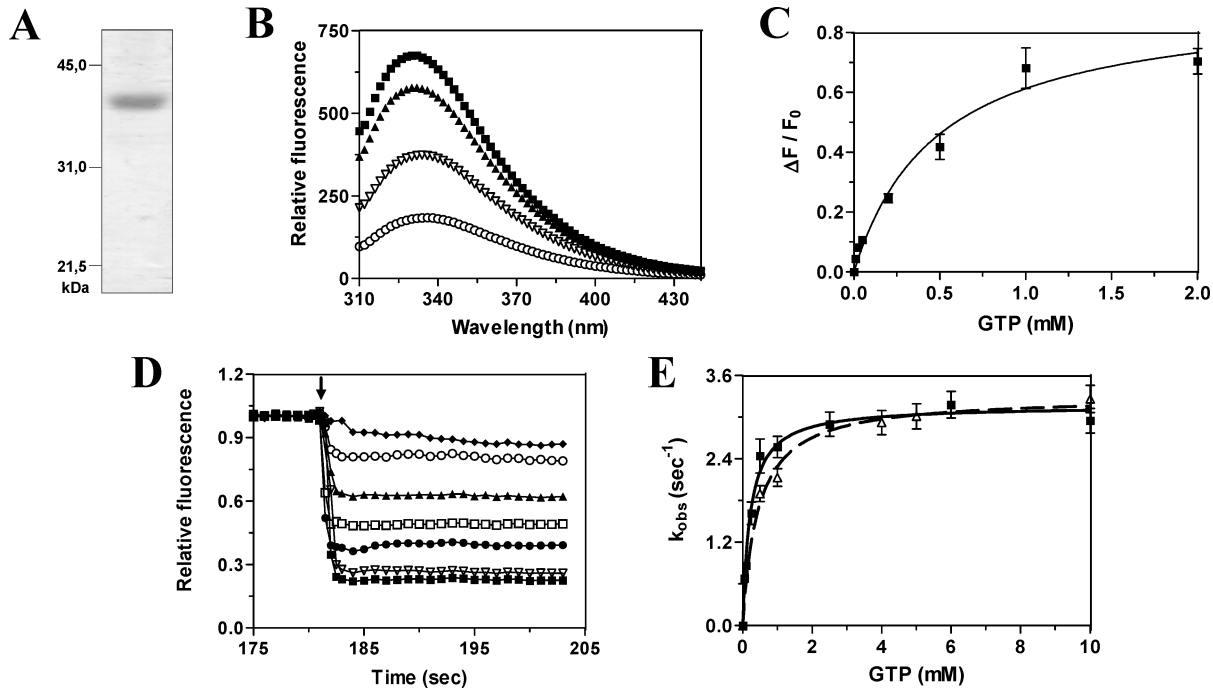

FIGURE 2: Binding of GTP to the A103R protein. (A) An aliquot of the purifed A103R protein was analyzed by electrophoresis through a 12.5% polyacrylamide gel containing 0.1% SDS and visualized by staining with Coomassie Blue dye. The positions and sizes (in kilodaltons) of the size markers are indicated. (B) Increasing amounts of GTP [0 μM (■), 50 μM (▲), 500 μM (▽), and 2 mM (○)] were added to a 10 μM solution of the enzyme in binding buffer [50 mM Tris-HCl and 50 mM KOAc (pH 7.5)], and the fluorescence emission spectrum was scanned from 310 to 440 nm. (C) A saturation isotherm can be generated from these data by plotting the change in fluorescence intensity at 332 nm as a function of added GTP. (D) Analysis of real-time binding of GTP to the A103R protein. A 10 μM solution of the enzyme was treated (↓) after 180 s with (◆) 50 μM, (○) 100 μM, (▲) 500 μM, (■) 1 mM, (●) 2.5 mM, (▽) 5 mM, or (■) 10 mM GTP. Excitation was performed at 290 nm, and emission was monitored for 45 s at 332 nm. (E) The observed initial rate constants (k_{obs}) were plotted as a function of added GTP in the absence (■) or presence (△) of 5 mM EDTA.

concentration of 12% and 0.75 mg/mL BSA. The mixtures in which reactions had been stopped were then allowed to precipitate on ice for 30 min and then centrifuged at 13000 rpm for 15 min. The supernatants were removed, and the pellets were washed with ethanol and centrifuged for 5 min at 13000 rpm. Again, the supernatants were removed, and samples were left to dry at room temperature for 15 min. The amount of remaining bound radioactive PP_i was measured by TriCarb 2200-CA liquid scintillation analyzer. The binding data were analyzed using a nonlinear least-squares one-site binding regression.

RNA Binding Assay. Reaction mixtures containing 50 mM Tris-HCl (pH 7.5), 10 mM NaCl, 100 nM EpG covalent intermediate, 50 mM EDTA, and increasing concentrations of [α-^{32}P]-capped, diphosphorylated, or triphosphorylated RNA (from 0.25 to 40 μM) were incubated at 30 °C for 30 min. Reaction samples were filtered on a 0.45 μm mixed cellulose membrane (Millipore), predamped with 1 mL of 50 mM Tris-HCl, and washed with 2 mL of 50 mM Tris-HCl. The membranes were recovered, and the radiolabeled RNA bound to the enzyme was monitored with a liquid scintillation counter.

RESULTS

Expression of A103R and Kinetic Pathway. To determine the complete kinetic parameters of the RNA guanylyltransferase reaction, a His-tagged version of the A103R protein was expressed in *E. coli* and purified by nickel−agarose chromatography (Figure 2A). The purified protein was then dialyzed in the presence of potassium pyrophosphate and magnesium to ensure a homogeneous nonguanylylated enzyme. The characterization of the kinetic parameters for the RNA guanylyltransferase reaction, which includes the interaction of the enzyme with GTP in the presence of a divalent cation to form a covalent intermediate EpG complex

Table 1: Equilibrium and Rate Constants

first step	$K_{D\cdot GTP}$ (mM)	0.50 ± 0.09
	$K_{D\cdot GTP-EDTA}$ (mM)	0.63 ± 0.15
	$K_{D\cdot PP_{i-1}}$ (mM)	0.09 ± 0.02
	k_1 (s^{-1} mM^{-1})	5.0 ± 0.5
	k_{-1} (s^{-1})	5.7 ± 0.4
	k_2 (s^{-1})	0.18 ± 0.01
	k_{-2} (s^{-1})	5.5 ± 0.6
second step	$K_{D\cdot PP_{i-2}}$ (mM)	0.10 ± 0.02
	$K_{D\cdot ppRNA}$ (μM)	3.3 ± 0.3
	$K_{D\cdot GpppRNA}$ (μM)	9.9 ± 0.5
	k_3 (s^{-1} μM^{-1})	0.37 ± 0.08
	k_{-3} (s^{-1})	1.1 ± 0.1
	k_4 (s^{-1})	0.0069 ± 0.0009
	k_{-4} (s^{-1})	0.00055 ± 0.00006
	k_{-5} (s^{-1})	1.9 ± 0.1
	k_5 (s^{-1} μM^{-1})	0.22 ± 0.04

with the concomitant release of pyrophosphate (step 1), and then the transfer of the GMP moiety to a diphosphorylated RNA end again in the presence of a divalent cation and further release of the capped RNA product (step 2), was undertaken with the purified recombinant A103R protein. Throughout this study, many reaction intermediates of the RNA guanylyltransferase reaction were isolated, and the kinetic and thermodynamic parameters involved in the transitions from one state to another were determined (Figure 1).

Interaction of GTP with A103R. Fluorescence spectroscopy was used to monitor the initial binding of GTP to the enzyme. Using the intrinsic fluorescence properties of the protein, we excited the A103R protein at a wavelength of 290 nm. Both tryptophans and tyrosines absorb at this wavelength (*15*). The protein in standard buffer at 25 °C produced a maximal peak of fluorescence emission at 332 nm (Figure 2B). The addition of GTP to the A103R protein resulted in a significant decrease in the fluorescence emission of the protein, which allowed us to monitor the association of GTP with A103R by measuring the variation of the fluorescence upon addition of increasing GTP concentrations (Figure 2B). It should be noted that free GTP in buffer did not produce any significant fluorescence emission when excited at 290 nm. Note that all fluorescence spectroscopy data were corrected for both dilution and inner filter effects. A $K_{D\cdot GTP}$ value of 0.50 ± 0.09 mM was determined for the binding of GTP to A103R (Figure 2C and Table 1). A similar constant, 0.63 ± 0.15 mM, was obtained in the presence of EDTA.

Real-time fluorescence spectroscopy assays were also performed to evaluate the rate constant for association of GTP with A103R. As shown in Figure 2D, increasing concentrations of GTP show an increase in the association rate as a function of the GTP concentration added. The initial rates of association for each curve were then estimated and plotted as a function of injected GTP concentrations (Figure 2E). An association rate constant (k_1) of 5.0 ± 0.5 s^{-1} mM^{-1} (Table 1) can be calculated from the initial slope of the generated data (*16*). It should be noted that this value is relatively low in comparison with the association rate constants typically obtained for the binding of substrates to enzymes (*17*). The rate of association of a protein with other macromolecules is significantly influenced by the geometry of the interaction and by electrostatic interactions. High association rates are typically associated with interactions between macromolecules that have complementary charged surfaces, while low association rates are usually encountered when only a small region of the protein is involved in the formation of the protein–ligand complex, which imposes a negative steric factor on the overall binding reaction. On the basis of the previous crystallization studies performed with the A103R protein, we envisage that the latter scenario likely applies to the binding of GTP to the active site of the enzyme in which the nucleotide binds to the active site located in a deep narrow cleft of the enzyme (*10*).

The A103R protein requires a divalent cation, either magnesium or manganese, to perform its activity (*9*). The involvement of the divalent cation in the binding of GTP to A103R was evaluated by performing similar fluorescence spectroscopy experiments in the presence of 5 mM EDTA. This was done to chelate the divalent ions that could be present in solution. The GTP association rate constant determined in the presence of EDTA was similar to the constant determined in the absence of EDTA (Figure 2E and Table 1), implying that no divalent cation is required for the initial binding of GTP to the enzyme. In addition, since magnesium or manganese is required for the catalytic actvity of the enzyme, we initially intended to assess the binding of magnesium to the A103R protein by real-time fluorescence spectroscopy. No changes in the fluorescence of A103R could be observed upon addition of up to 50 mM $MgCl_2$ to the enzyme (data not shown). We conclude that, in agreement with previous studies (*10, 13*), the divalent cation cofactor required for activity does not bind to the apoenzyme, but only to the protein following the binding of GTP.

We then sought to evaluate the dissociation rate constant (k_{-1}) for GTP using a simple competition experiment. An excess of unlabeled GTP was added to the E·GTP intermediate, and the dissociation was monitored as a function of time, by stopping the reaction at various times with TCA precipitation (Figure 1 of the Supporting Information). To obtain a satisfying dissociation rate constant, we used a large excess of competitive GTP. An excess of 100-fold unlabeled GTP versus radiolabeled GTP was used in this assay, and a k_{-1} value of 5.7 ± 0.4 s^{-1} was obtained (Table 1). In fact, a 20-fold excess was enough to obtain a maximal dissociation (data not shown). It should be noted that time points under 0.5 s proved to be technically impossible to measure with consistency. However, we are confident that the rate constants obtained by this method are relevant (compared with the fluorescence spectroscopy data), since there is an only 2−2.5-fold variation between the calculated ($K_D = k_{-1}/k_1$) and experimentally determined constants for the binding of GTP to the enzyme.

Inhibition of the First-Step Forward Reaction by Pyrophosphate. The presence of pyrophosphate in solution has been shown to strongly inhibit the forward RNA guanylyltransferase reaction (*9*). We therefore decided to investigate the binding of pyrophosphate to the A103R protein. To monitor the binding of pyrophosphate to the A103R protein, radiolabeled pyrophosphate was generated as described in Materials and Methods. The A103R protein was incubated in the presence of increasing radiolabeled pyrophosphate concentrations and then precipitated using trichloroacetic acid (TCA). The pellets were washed, and the radioactive counts were determined for each pyrophosphate concentration. A $K_{D\cdot PP_{i-1}}$ value of 0.09 ± 0.02 mM was determined for the binding of pyrophosphate to the enzyme (Figure 3A), indicating that the protein has a 5-fold higher affinity for

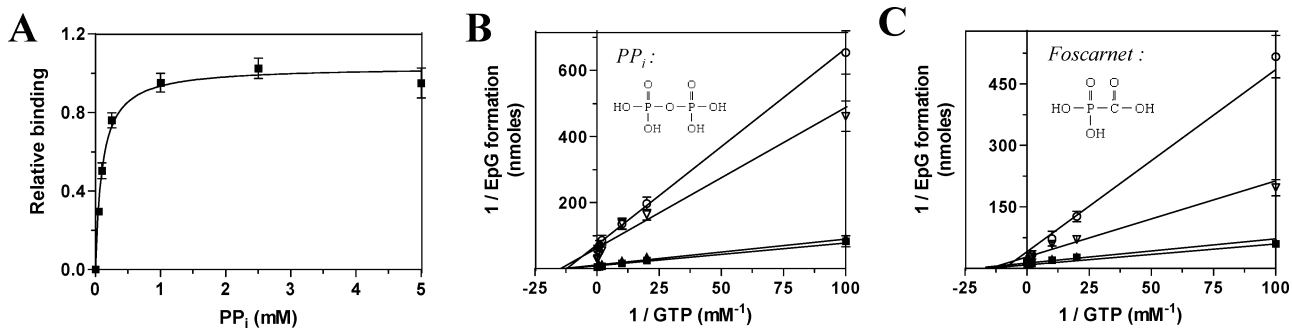

FIGURE 3: Binding of pyrophosphate by A103R. (A) Increasing amounts of radiolabeled PP_i were added to a 10 μM solution of the A103R protein, and the radioactive counts after TCA precipitation were evaluated and plotted as a function of the PP_i concentration. (B) Double-reciprocal plot of the inhibition of EpG formation in the presence of 0 μM (■), 50 μM (▲), 1 mM (▽), and 5 mM (○) pyrophosphate in solution. (C) Double-reciprocal plot of the inhibition of EpG formation in the presence of 0 μM (■), 500 μM (▲), 1 mM (▽), and 5 mM (○) foscarnet.

pyrophosphate versus GTP (Table 1). Note that control precipitation experiments were performed with pyrophosphate alone.

We then carried inhibition kinetic assays in which the reactants for the RNA guanylyltransferase reaction were incubated in the presence of various initial pyrophosphate concentrations. Formation of the enzyme−GMP complex was monitored as a function of GTP concentration in the presence of increasing amounts of pyrophosphate. A significant decrease in the V_{max} is observed even at low pyrophosphate concentrations, while the K_m remains constant (Table 1 of the Supporting Information). The inhibition of the reaction by pyrophosphate was shown to be noncompetitive with an associated $K_{i\text{-}PP_i}$ of 0.8 mM (Figure 3B). For an equimolar concentration of GTP and pyrophosphate (1 mM each), an inhibition of ~75% of the maximal level of complex formation is produced. The $K_{i\text{-}PP_i}$ obtained is a log higher than the $K_{D\cdot PP_i}$, most likely because in the presence of GTP the enzyme can undergo a conformational change that shields the PP_i binding site, weakening its binding ability. We also evaluated the ability of a pyrophosphate analogue, foscarnet, to inhibit the RNA guanylyltransferase reaction. The same assays were carried out using various concentrations of foscarnet, and noncompetitive inhibition with a $K_{i\text{-}fosc}$ of 2.0 mM was observed (Figure 3C and Table 1 of the Supporting Information). Again, a noteworthy inhibition is obtained by addition of an increasing concentration of this compound, and an inhibition of 30% of the maximal level of complex formation is observed for equimolar concentrations of GTP and foscarnet in solution. We conclude that foscarnet is a potent inhibitor of the RNA guanylyltransferase reaction, albeit to a lesser extent than pyrophosphate.

Kinetics of the First-Step Forward Reaction. The forward reaction was initially investigated under two different conditions, one in which the protein was added last to enable the reaction to occur and the other in which the enzyme was allowed to bind to GTP and undergo any needed conformational change before the addition of the magnesium which is required for the reaction. The plots obtained in the presence of 10 μM GTP showed that the initial rate of reaction at 30 °C is the same whether the enzyme was previously bound to GTP (Figure 2 of the Supporting Information), indicating that the limiting step at this temperature is the catalytic part of the reaction and that both the rates of GTP binding and the conformational change are negligible in comparison.

We then intended to evaluate the kinetic parameters of this reaction. As observed in previous studies, the RNA guanylyltransferase reaction is relatively inefficient (*3*). This lack of efficiency can be attributable in part to the inhibition of the first step by the pyrophosphate reaction product. Moreover, previous studies have not always used pyrophosphate in their dialysis purification protocols to ensure that the enzyme was in the apoenzyme form before kinetic characterization (*3, 9*). While trying to perform kinetic assays with the A103R protein, where we monitored the use of radiolabeled GTP for formation of an EpG complex as a function of time, we observed only a small amount of product formation that was constant over time (Figure 3A of the Supporting Information). The same experiment performed in the presence of 1.25 μg/mL pyrophosphatase yielded more satisfying results, showing both an increase in the level of complex formation and a complete use of the radiolabeled GTP as a function of time (Figure 3B of the Supporting Information).

The kinetic constants for the first step of the RNA guanylyltransferase reaction were evaluated by radioactive assays in which the formation of EpG as a function of time could be monitored following SDS−PAGE (Figure 4A). All the first-step forward reaction kinetic assays were conducted in the presence of pyrophosphatase to ensure that the reaction was driven in the desired forward direction. Moreover, the constants are obtained in a single-turnover environment since the enzyme is covalently bound to GMP at the end of the reaction and is not available for another round of catalysis. GTP concentrations ranging from 0.1 to 50 times the concentration of enzyme were used in this assay. It should be noted that some of the reactions performed at lower GTP concentrations (1–25 μM) did not reach the same end point since the GTP concentrations used in these assays were significantly lower than the K_D value for the GTP substrate. We calculated the relative quantity of complex formation for various initial GTP concentrations (Figure 4B), and the initial rates derived from the plots of each of the latter GTP concentrations were plotted as a function of their corresponding initial GTP concentrations, yielding a first-order rate constant (Figure 4C). We determined an apparent Michaelis–Menten (K_m') value of 10.5 ± 2.5 μM and an apparent maximal velocity (V_{max}') of 0.07 ± 0.01 nmol s^{-1} for this forward reaction. Interestingly, the apparent K_m value determined in the presence of pyrophosphatase is 50-fold

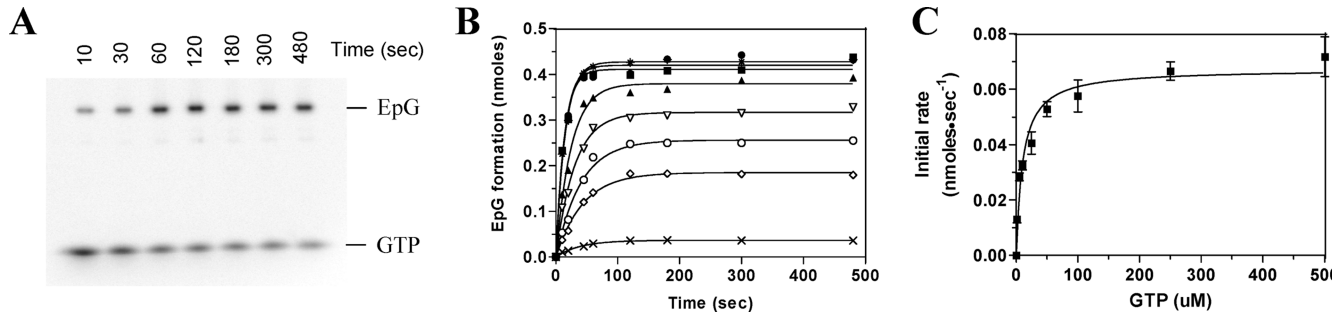

FIGURE 4: A103R first-step forward reaction kinetics. (A) Typical SDS−PAGE for monitoring EpG formation by use of [α-^{32}P]GTP in solution from 10 to 480 s. Autoradiographical quantification of these bands provides data for the kinetic activity of A103R. (B) Plots derived from SDS−PAGE quantification of the activity of 10 μM A103R in the presence of 1 (×), 5 (◇), 10 (○), 25 (▽), 50 (▲), 100 (■), and 500 μM (●) [α-^{32}P]GTP in solution. (C) Plot of the initial rates of reaction obtained for each of the curves found in panel B as a function of GTP concentration.

lower than the measured $K_{D\text{-}GTP}$. A likely explanation for the observation that the apparent K_m value is smaller than the K_D value is that the uptake of GTP is probably fast relative to the reappearance of the unoccupied binding site during catalysis. Structural studies have demonstrated that following the initial binding of GTP to the open form of the enzyme, a conformational change is required to promote the binding of the essential divalent cation by promoting the closure of the enzyme. This conformational rearrangement is then followed by the transfer of a phosphoryl group from GTP to produce the GMP−enzyme covalent complex. Finally, the cleavage of GTP destabilizes the closed form of the enzyme which opens again to release the pyrophosphate. All these conformational changes are likely to contribute to the low rate of reappearance of the unoccupied GTP binding site.

Pyrophosphate Binding and Kinetics of the First-Step Reverse Reaction. Since the reverse reaction of the first step requires pyrophosphate to occur and the latter can bind to the enzyme alone, we also determined the affinity of PP_i for the preformed EpG complex. We therefore incubated the EpG complex in the presence of increasing radiolabeled pyrophosphate concentrations and used TCA precipitation to evaluate the amount of radiolabeled PP_i bound to the complex. A $K_{D\cdot PP_{i-2}}$ value of 0.10 ± 0.02 mM (Figure 4A of the Supporting Information) could be determined for the binding of pyrophosphate to the EpG complex (Table 1). This constant is similar to the one obtained for the binding of PP_i to the enzyme alone, suggesting that the pyrophosphate does not bind the enzyme at the same site as GTP or GMP.

The kinetic constants were then calculated for the reverse reaction of the first step of the RNA guanylyltransferase reaction. This time, we used the purified EpG complex and quantified the release of GTP as a function of time in the presence of various initial pyrophosphate concentrations (Figure 4B of the Supporting Information). In light of the previous results cited above, we assumed that the forward RNA guanylyltransferase reaction is negligible compared to the reverse reaction we were monitoring. Again, we obtained a pseudo-first-order rate constant (Figure 4B of the Supporting Information) which revealed an apparent K_m' value of 2.6 ± 1.1 μM and an apparent V_{max}' of 0.35 ± 0.04 nmol s^{-1} for the reverse reaction. The reverse reaction K_m is 4-fold lower than the corresponding constant for the forward reaction, while the maximal rate of reaction is 5-fold higher, suggesting that the reverse reaction can produce its activity both with a lower concentration of reactant and at a higher rate. Moreover, using the equation $k_{cat} = V_{max}/[E]$, we calculated a k_2 value of 0.18 ± 0.01 s^{-1} and a k_{-2} value of 5.5 ± 0.6 s^{-1} (Table 1), demonstrating that the catalytic activity of the reverse reaction occurs at a rate 40-fold higher than that of the forward RNA guanylyltransferase reaction. The k_{cat}/K_m' values for the forward and reverse reactions (1.7 × 10^4 and 2.1 × 10^6 M^{-1} s^{-1}, respectively) also outline that the reverse reacton occurs at a higher rate.

Association of Diphosphorylated RNA with EpG and Dissociation from EpG. Filter binding assays were used to monitor both the rate of association of ppRNA to the EpG complex and the equilibrium constant for this interaction. The selected nitrocellulose membranes (0.45 μm mixed cellulose membrane, Millipore) possess an overall negative charge, therefore allowing binding of positively charged proteins and repulsion of the negatively charged RNAs. Interaction of radiolabeled ppRNA with the membranes could not be detected, whereas the radioactivity counts increased linearly with the quantity of protein in solution (data not shown). This assay allowed us to evaluate an equilibrium constant ($K_{D\cdot ppRNA}$) of 3.3 ± 0.3 μM (Figure 5A and Table 1) by adding increasing amounts of ppRNA to the EpG complex. An association rate constant (k_3) of 0.37 ± 0.08 s^{-1} μM^{-1} (Figure 5B and Table 1) could also be calculated by halting these reactions with filtration at various times and plotting each of their observed association rates as a function of the initial ppRNA concentration. These experiments were conducted in the presence of EDTA, suggesting, as for the first step of the reaction, that the interaction is ion-independent.

The dissociation rate constant (k_{-3}) for dissociation of the ppRNA from the EpG complex was also evaluated using this method. As for the dissociation of GTP, an excess of cold ppRNA was added to the EpG•ppRNA intermediate, and the dissociation is monitored as a function of time (Figure 5C). In this case, we used a 50-fold excess of unlabeled ppRNA versus radiolabeled ppRNA, and we obtained a k_{-3} value of 1.1 ± 0.1 s^{-1} (Table 1). We can observe that the dissociation of ppRNA from the EpG complex occurs at a 3-fold higher rate than its association, suggesting a poor association of the disphosphorylated RNA with EpG. We believe this high dissociation rate is necessary for an effective release of the final RNA product of reaction. Moreover, it should be noted that all the experimental parameters independently determined for the interaction of

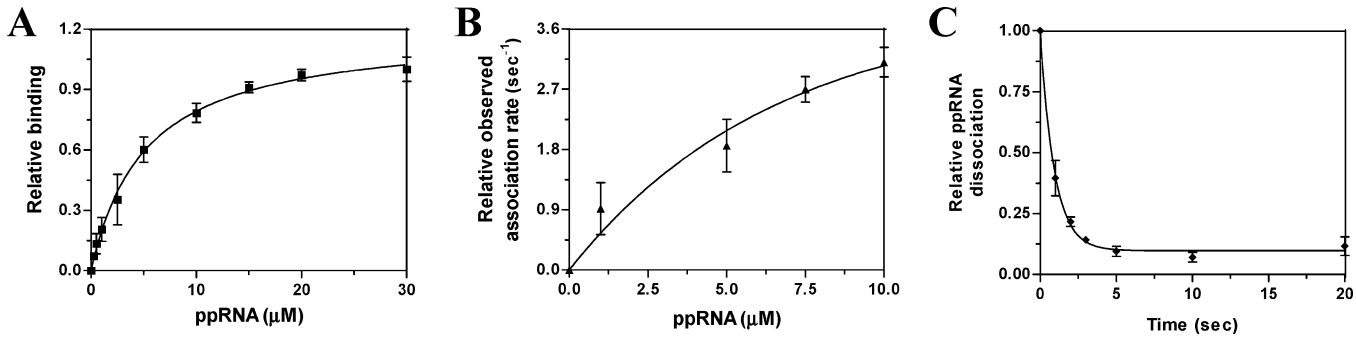

FIGURE 5: Interaction of diphosphorylated RNA with the EpG complex. (A) Increasing concentrations of diphosphorylated RNA (ppRNA) were added to a 5 μM EpG complex solution with EDTA. The plot of the binding as a function of added RNA concentration, from which the equilibrium binding constant for binding of ppRNA to EpG was derived, is shown. (B) Analysis of real-time binding of ppRNA to EpG was conducted, and the observed initial rate constants (k_{obs}) for each RNA concentration (1, 2.5, 5, 7.5, and 10 μM) were plotted as a function of the amount of added ppRNA. (C) Dissociation of [^{32}P]ppRNA as a function of time from the EpG complex, evaluated by the addition of a 50-fold excess of unlabeled ppRNA.

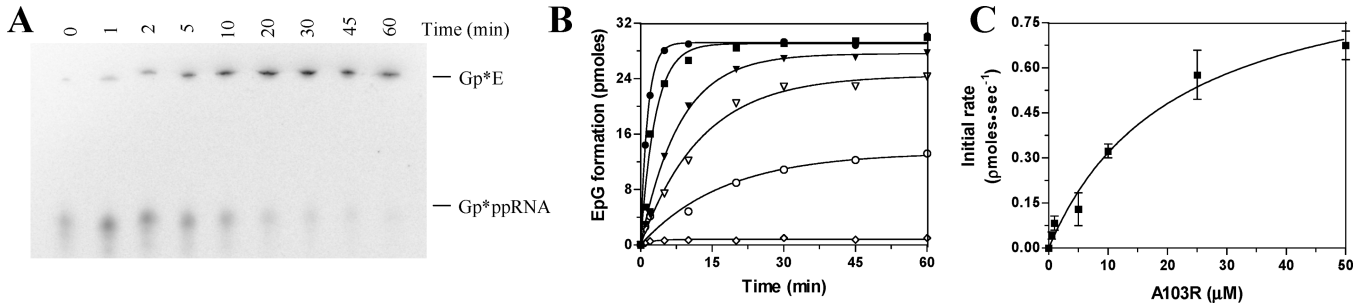

FIGURE 6: A103R second-step reverse reaction kinetics. (A) Typical polyacrylamide gel for the monitoring of EpG formation by addition of E to [^{32}P]GpppRNA in solution from 0 to 60 min. Quantification of these bands provides the kinetic data to be analyzed. (B) Plots derived from polyacrylamide gel quantification of the activity of 0.1 (◇), 0.5 (○), 1 (▽), 5 (▼), 10 (■), and 50 μM (●) A103R on 1 μM [^{32}P]GpppRNA. (C) Plot for the initial rates of the reaction obtained for each of the curves found in panel B as a function of enzyme (A103R) concentration.

the enzyme with the diphosphorylated RNA substrate evaluated using the same technique (filter binding assay) are consistent with the general formula $K_D = k_{-3}/k_3$, highlighting the consistency of the experimental approach.

Second-Step Forward Reaction. To evaluate the kinetics of the forward reaction for the second step of the RNA guanylyltransferase reaction, we produced a diphosphorylated RNA substrate and radiolabeled EpG complex. We chose an RNA sequence from the PBCV-1 DNA polymerase gene that would correspond to the 5′ portion of the transcribed mRNA of the gene. We were able to monitor the transfer of radiolabeled GMP to the RNA as the capping reaction occurred to produce capped RNA (GpppRNA) (Figure 5A of the Supporting Information). By monitoring the reaction as a function of time for various RNA concentrations (Figure 5B of the Supporting Information), we were able to evaluate the initial rates of reaction for each concentration. By plotting these initial rates as a function of the amount of added diphosphorylated RNA in solution, we calculated a K_m' value of 3.6 ± 1.0 μM and a V_{max}' of 1.23 ± 0.26 pmol min^{-1} (Figure 5C of the Supporting Information). The K_m' is similar to the K_D measured for the interaction with diphosphorylated RNA, suggesting the binding of RNA to the enzyme (and not the transfer of the GMP moiety to the RNA) is the limiting step of this catalytic step.

Second-Step Reverse Reaction. We then sought to investigate the kinetics of the reverse catalytic activity of the second step of the RNA guanylyltransferase reaction. To ensure that we would be monitoring this reaction at its full potential, antarctic phosphatase was added to the reaction mixture. This enzyme is able to dephosphorylate tri-, di-, and monophosphorylated RNAs but is unable to cleave a cap structure. Therefore, we were able to drive the reverse reaction by depleting the diphosphorylated RNA product of the reaction with the antarctic phosphatase (data not shown).

Morever, this kinetic analysis was not conducted by adding various concentrations of the GpppRNA substrate but by varying the enzyme concentration, because the substrate concentrations required for the maximal reaction rate could not be obtained. In a single-turnover environment, both methods should yield the same initial rates. We indeed proved experimentally that the evaluated initial rates corresponded when either the GpppRNA or the enzyme concentration was varied (data not shown). We therefore assumed that the constants calculated for this reverse reaction can be compared to the other evaluated constants of the RNA guanylyltransferase reaction.

A radiolabeled GpppRNA substrate was synthesized by the forward reaction of the second step of the RNA guanylyltransferase using radiolabeled GMP. The transfer of this GMP moiety back to the enzyme was monitored as a function of time, for increasing E concentrations in solution, to evaluate the kinetics of the reverse reaction (Figure 6A,B). Again, the initial rates for each enzyme concentration were plotted as a function of the added A103R protein concentration, allowing us to calculate a K_m' value of 21.2 ± 5.7 μM and a V_{max}' of 0.99 ± 0.12 pmol min^{-1} (Figure 6C). The k_{cat}/K_m' values were calculated for the forward and reverse reactions of this second step, yielding values of 5.6 × 10^6 and 5.5 × 10^5 M^{-1} s^{-1}, respectively. We can conclude, with

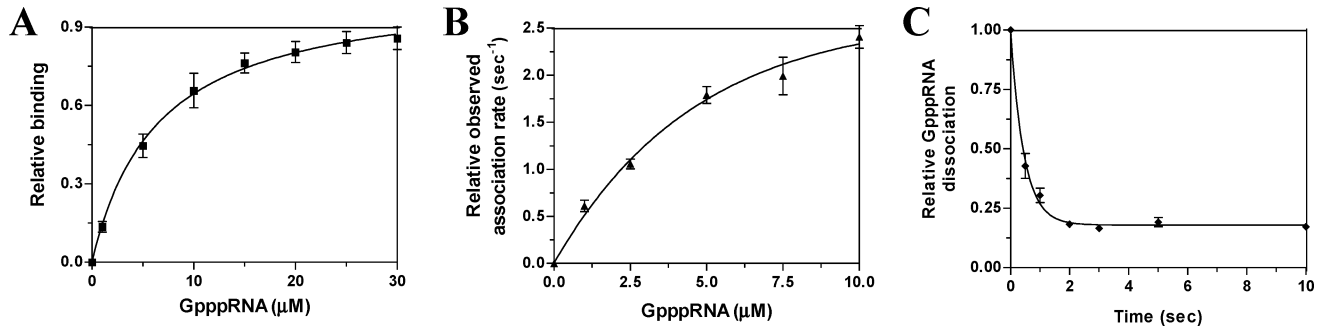

FIGURE 7: Interaction of capped RNA with A103R. (A) Increasing concentrations of capped RNA (GpppRNA) were added to a 5 μM A103R solution with EDTA. The plot of the binding as a function of added RNA concentration is shown. (B) Analysis of real-time binding of GpppRNA to the enzyme was carried out, and the observed initial rate constants (k_{obs}) for each RNA concentration (1, 2.5, 5, 7.5, and 10 μM) were plotted as a function of the amount of added GpppRNA. (C) Dissociation of [^{32}P]GpppRNA as a function of time from the EpG complex, evaluated by the addition of a 50-fold excess of unlabeled GpppRNA.

the K_m' and k_{cat}/K_m' values for the forward and reverse reactions, that the affinity of the A103R protein for the final product of the reaction is lower. Furthermore, the catalytic constants for these reactions indicate that the forward reaction has a 12-fold higher rate of catalysis than the reverse reaction.

Release of the Capped RNA. The final step of the capping reaction is the release of the capped RNA product. It was previously shown that the overall RNA guanylyltransferase reaction is fully reversible (*3*), and with our reverse kinetics assays, it was clear that the enzyme could associate with the final product of the reaction. We therefore sought to evaluate the dissociation of the GpppRNA from the enzyme, but also its association and the equilibrium constant of this interaction. As for the binding of diphosphorylated RNA to the EpG complex, we used filter binding assays to measure these various kinetic constants. A $K_{D\cdot GpppRNA}$ of 9.9 $\pm$ 0.5 μM (Figure 7A and Table 1) was measured by adding increasing amounts of GpppRNA to the enzyme alone. The association was then monitored as a function of time for these concentrations of capped RNA, yielding an association rate constant (k_5) of 0.22 $\pm$ 0.12 s^{-1} μM^{-1} (Figure 7B and Table 1). The dissociation rate constant (k_{-5}) was evaluated by adding a 50-fold excess of cold GpppRNA to the E·GpppRNA intermediate, and the dissociation was monitored as a function of time (Figure 5C). A k_{-5} value of 1.9 $\pm$ 0.1 s^{-1} was obtained (Table 1). Again, a perfect concordance is observed between the K_D value and both the association and dissociation rates ($K_D = k_{-1}/k_1$). As for previous binding experiments, EDTA was used in each of these reactions to ensure that no catalytic activity would occur and that only the binding of RNA was assessed. We can observe with the equilibrium constant that A103R has 3-fold less affinity for the GpppRNA product of the reaction than the diphosphorylated RNA substrate of the second step of the RNA guanylyltransferase reaction. Furthermore, the dissociation rate is increased by 2-fold, favoring the release of the final product.

DISCUSSION

The addition of a cap structure at the 5′ end of eukaryotic mRNAs is one of the major modifications that occur during RNA processing (*1, 2*). Many viruses encode their own capping machinery to synthesize viral mRNAs harboring the cap structure (*4*). Viral enzymes involved in the formation of the 5′-terminal cap structure have been extensively characterized in recent years, and the elucidation of crystallographic structures provided numerous insights into the reaction pathway (*10, 13*). Although these studies have been very instructive, the complete parameters of the various kinetic pathways have not been thoroughly investigated. In an effort to gain further knowledge about the RNA guanylyltransferase reaction, we performed fluorescence spectroscopy, radioactive kinetics, and filter binding assays to evaluate the kinetic parameters of the complete RNA guanylyltransferase reaction.

This presents a thorough quantitative analysis of the kinetics involved during the RNA guanylyltransferase reaction. A thermodynamic scheme for the progress of the reaction was generated as a function of the energies involved in each step (Figure 8). Analysis of the thermodynamic data for the first step of the reaction indicates that the RNA capping enzyme is thermodynamically more stable when bound to GTP (−4.5 kcal mol^{-1}). Both the apoenzyme and the enzyme covalently linked to GMP (−2.4 kcal mol^{-1}) are less stable in terms of free energy. We hypothesize that the enzyme covalently linked to GMP is thermodynamically less stable because it is required in the second step of the RNA capping reaction which entails the catalytic transfer of the GMP moiety to the diphosphate end of the RNA. Analysis of the crystal structure of the PBCV-1 RNA guanylyltransferase has previously provided evidence of important conformational changes that occur during both substrate binding and reaction chemistry, most notably, the opening and closing of the gap between the N- and C-terminal domains (*10, 13*). The conformational change is required for the catalytic formation of the covalent enzyme−GMP intermediate, since only in the closed conformation is the enzyme able to bind the metal ion cofactor and undergo catalysis and form the covalent enzyme−GMP intermediate (*10, 13*). We therefore hypothesize that the stability of the E·GTP intermediate is likely due to the conformational change of the enzyme that occurs after GTP binding. Interestingly, previous denaturation studies performed with the *Saccharomyces cerevisiae* RNA guanylyltransferase have also noted the increased stability of the enzyme−GMP intermediate (*18*).

The thermodynamics of the second step of the RNA guanylyltransferase reaction indicate that the enzyme experiences a series of less stable intermediates before terminating the reaction at a more favorable level of energy (−0.9 kcal mol^{-1}). The EpG complex bound to diphosphorylated RNA (EpG·ppRNA) and the enzyme bound to capped RNA

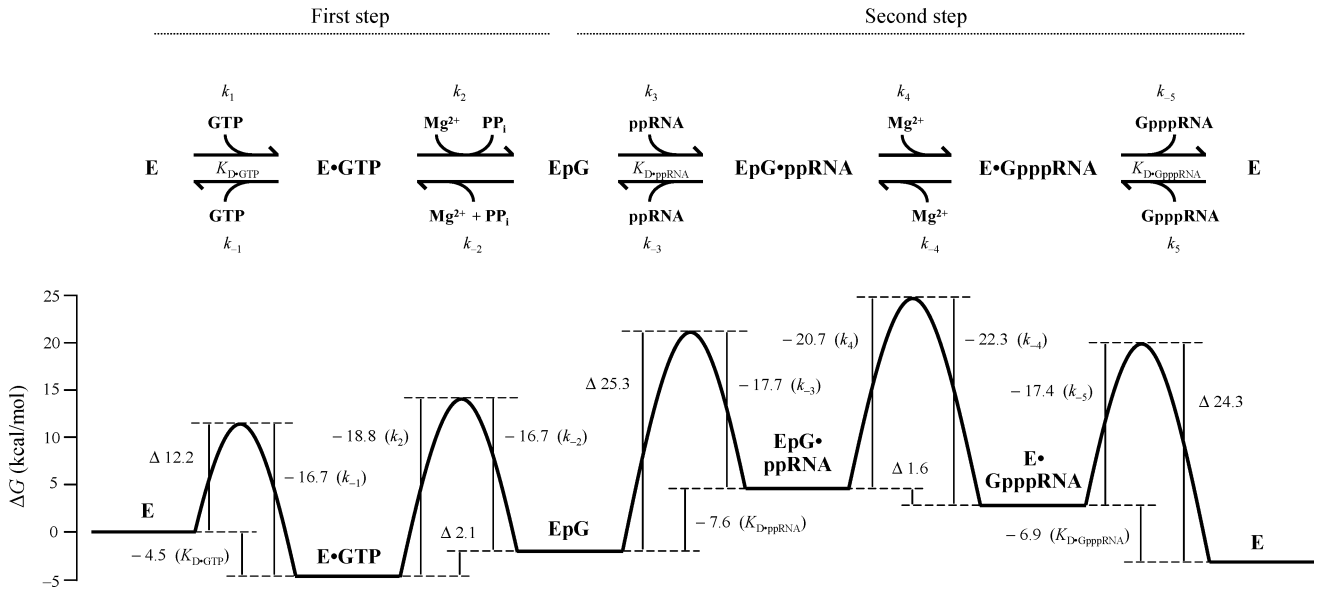

FIGURE 8: Gibbs free energy profile for the RNA guanylyltransferase reaction. Gibbs free energies are graphically shown in a representation of our suggested reaction pathway for the overall RNA guanylyltransferase reaction. The free energies (ΔG) were calculated using the equation $\Delta G = RT \ln K$, where $T = 303$ K (30 °C), $R = 1.987$ cal K^{-1} mol^{-1}, and K is either the observed equilibrium constant or the constant calculated using the equation $k = (K_b T/h)K^*$, where k is a rate constant, K_b is the Boltzmann constant, $T = 303$ K (30 °C), h is Planck's constant, and K^* is the estimated equilibrium constant. ΔG values are presented with the constant used for calculation. The values preceded by a delta (Δ) were calculated by addition or subtraction of other ΔG values and not from kinetic constants.

(E•GpppRNA) are the two intermediates with the highest free energies of the whole reaction, in contrast with the intermediates of the first part of the RNA guanylyltransferase reaction which are very stable in comparison. The first step is very dynamic with low energy variations between the intermediates. The binding of diphosphorylated RNA by the EpG complex, initiating the second step of the reaction, is the overall energetically limiting step of the RNA guanylyltransferase reaction with its $\Delta = 25.3$ kcal mol^{-1}requirement (Figure 8). We believe that the association of the A103R protein with diphosphorylated RNA will be less limiting in a cellular context since the RNA 5′-triphosphatase, responsible for the catalysis of the first step of the cap formation, and the RNA guanylyltransferase are known to interact with the CTD of the polymerase II during transcription (*19–22*). The RNA 5′-triphosphatase synthesizes the diphosphorylated RNA which is then used by the associated RNA guanylyltransferase, overcompensating for the RNA binding limitation of the RNA guanylyltransferase reaction.

For the reverse mechanism, the limiting step is the binding of the capped RNA to the free enzyme, with a $\Delta = 24.3$ kcal mol^{-1} energy requirement (Figure 8). Once the capped RNA is bound, the enzyme is able to undergo catalysis to re-create the EpG complex and release diphosphorylated RNA. However, we believe that this activity will not occur in vivo since the capped RNA will be recognized by cap binding proteins after its synthesis, preventing further interaction with the RNA guanylyltransferase (*23*).

Overall, our thermodynamic analyses clearly showed that the first step of the RNA guanylyltransferase is very dynamic, as indicated both by the respective ΔG values for the different forms of the enzyme and by the reversibility of each part of the reaction. In contrast, we showed that the second step comprises the limiting steps for both the direct and reverse overall reactions. In both cases, the binding to the RNA substrates is the step requiring the highest energy, and generating unstable intermediates that will promote the catalytic activites. The first step of the reaction is favored in terms of free energy with a final intermediate (E•GTP) −2.4 kcal mol^{-1} below the energy of the apoenzyme. The second step is also driven forward by a final free energy that is −0.9 kcal mol^{-1} lower than its initial starting point. The overall reaction ends up with a 3.3 kcal mol^{-1} decrease in free energy when performed in vitro at 30 °C (Figure 8).

The PBCV-1 RNA guanylyltransferase belongs to an enzyme superfamily of covalent mononucleotidyltransferases, which includes both DNA and RNA ligases (*11*). The members of this family contain a conserved active site motif (KxDG) in which the lysine residue is involved in the formation of the enzyme−GMP (capping) or enzyme−AMP (ligases) intermediate (*11*). The crystal structures of five different members of this important family have been determined, providing insightful information about the reaction chemistry (*10, 13, 21, 24*). Members of this family are characterized by a common tertiary structure that consists of an N-terminal domain, which encompasses the nucleotide-binding pocket, and a C-terminal oligonucleotide binding fold domain. The RNA guanylyltransferase from reovirus can also form an enzyme−GMP covalent intermediate involving a lysine residue (*25*), but its structure is completely different from those of the eukaryotic and viral guanylyltransferases of the mononucleotidyltransferase family (*26*). We hypothesize that the energetic profile that we have determined for the PBCV-1 RNA guanylyltransferase reaction is likely to apply to other members of this family. Specific mutations have been shown to affect GTP binding, formation of the EpG complex, and transfer of GMP to diphosphorylated RNA in *S. cerevisiae*, vaccinia virus, and the human capping enzymes (*27–29*). The corresponding mutations could eventually be used with the PBCV-1 RNA guanylyltransferase to emphasize the similarities between these members of the nucleotidyltransferase family. Moreover, it will be interesting to investigate the energetics involved in the capping of viral

mRNAs from other classes of guanylyltransferases. For instance, the nsP1 protein of Semliki Forest virus methylates the N7 position of GTP to generate ^{m7}GTP, before subsequently transferring the ^{m7}GMP moiety to the 5′ diphosphate end of the viral mRNAs (*30*). Such a guanylylation pathway has also been observed for other members of the alphavirus-like superfamily such as hepatitis E virus, tobacco mosaic virus, brome mosaic virus, and bamboo mosaic virus (*31–34*). Significant differences in the free energies of the different forms of these RNA guanylyltransferases are likely to exist because of the presence of an additional intermediate during the RNA guanylyltransferase reaction.

During the characterization of the RNA guanylyltransferase reaction, we observed that foscarnet had the ability to inhibit the forward reaction of the first step of the reaction. This analogue of pyrophosphate is currently used against herpesvirus infections, mainly cytomegalovirus, and has been shown to be relatively effective against hepatitis B virus (HBV) and human immunodeficiency virus (HIV) (*35, 36*). The precise mechanism of action of this drug remains elusive, although it has been proposed that the pyrophosphate analogue could bind close to the active center of viral polymerases, thereby inhibiting the pyrophosphate exchange reaction (*37*). In the study presented here, foscarnet produced a significant inhibition of the activity of A103R in vitro. Interestingly, the enzyme was also able to use foscarnet for the first-step reverse reaction, creating a novel GDP−COOH product (data not shown). Subsequent in vivo studies performed in the presence of foscarnet should eventually indicate whether the antiviral can efficiently inhibit the capping of viral mRNAs.

This study represents the first thorough kinetic and thermodynamic characterization of the mechanism of a capping enzyme and highlights the energetics involved in the RNA guanylyltransferase reaction. Although our knowledge of the different mechanisms involved in RNA capping is still incomplete, we believe that the characterization of the kinetic and thermodynamic parameters involved in the individual steps required for the synthesis of the RNA cap structure is critical in understanding the overall reaction chemistry. These studies add another dimension to the high-resolution structural studies that have revealed key insights into the structural requirements for each of the individual steps. Given the recent interest in the development of selective inhibitors that can be used as antiviral agents, understanding the energetics of protein involved in the RNA capping reaction is critically important.

SUPPORTING INFORMATION AVAILABLE

Kinetic parameters for the inhibition of the first step of the RNA guanylyltransferase reaction (Table 1), GTP dissociation rate constants (Figure 1), the limiting step of the first part of the RNA guanylyltransferase reaction (Figure 2), the RNA guanylyltransferase reaction (Figure 3), A103R first-step reverse reaction kinetics (Figure 4), and A103R second-step forward reaction kinetics (Figure 5). This material is available free of charge via the Internet at http://pubs.acs.org.

REFERENCES

1. Shuman, S. (2000) Structure, mechanism, and evolution of the mRNA-capping apparatus. *Prog. Nucleic Acids Res. Mol. Biol. 66*, 1–40.
2. Furuichi, Y., and Shatkin, A. J. (2000) Viral and cellular mRNA capping: Past and prospects. *Adv. Virus Res. 55*, 135–184.
3. Venkatesan, S., and Moss, B. (1981) Eukaryotic mRNA capping enzyme-guanylate covalent intermediate. *Proc. Natl. Acad. Sci. U.S.A. 79*, 340–344.
4. Shuman, S. (1990) Catalytic activity of vaccinia mRNA capping enzyme subunits coexpressed in *Escherichia coli*. *J. Biol. Chem. 265*, 11960–11966.
5. Babich, A., and Nevins, J. R., Jr. (1980) Early capping of transcripts from the adenovirus major late transcription unit. *Nature 287*, 246–248.
6. Plotch, S. J., Bouloy, M., Ulmanen, I., and Krug, R. M. (1981) A unique cap(^{m7}GpppXm)-dependent influenza virion endonuclease cleaves capped RNAs to generate the primers that initiate viral RNA transcription. *Cell 23*, 847–858.
7. Van Etten, J. L., Lane, L. C., and Meints, R. H. (1991) Viruses and virus-like particles of eukaryotic algae. *Microbiol. Rev. 55*, 586–620.
8. Ho, C. K., Gong, C., and Shuman, S. (2001) RNA triphosphatase component of the mRNA capping apparatus of *Paramecium bursaria Chlorella* virus 1. *J. Virol. 75*, 1744–1750.
9. Ho, C. K., Van Etten, J. L., and Shuman, S. (1996) Expression and Characterization of an RNA Capping Enzyme Encoded by *Chlorella* Virus PBCV-1. *J. Virol. 70*, 6658–6664.
10. Hakansson, K., Doherty, A. J., Shuman, S., and Wigley, D. B. (1997) X-ray crystallography reveals a large conformational change during guanyl transfer by mRNA capping enzymes. *Cell 89*, 545–553.
11. Cong, P., and Shuman, S. (1993) Covalent catalysis in nucleotidyl transfer. A KTDG motif essential for enzyme-GMP complex formation by mRNA capping enzyme is conserved at the active sites of RNA and DNA ligases. *J. Biol. Chem. 268*, 7256–7260.
12. Wang, S. P., Deng, L., Ho, C. K., and Shuman, S. (1997) Phylogeny of mRNA capping enzymes. *Proc. Natl. Acad. Sci. U.S.A. 94*, 9573–9578.
13. Hakansson, K., and Wigley, D. B. (1998) Structure of a complex between a cap analogue and mRNA guanylyl transferase demonstrates the structural chemistry of RNA-capping. *Proc. Natl. Acad. Sci. U.S.A. 95*, 1505–1510.
14. Bisaillon, M., and Bougie, I. (2003) Investigating the roles of metal ions in the catalytic mechanism of the yeast RNA triphosphatase. *J. Biol. Chem. 36*, 33963–33971.
15. Painter, G. R., Wright, L. L., Hopkins, S., and Furmanm, P. A. (1991) Initial binding of 2′-deoxynucleoside 5′-triphosphates to human immunodeficiency virus type 1 reverse transcriptase. *J. Biol. Chem. 266*, 19362–19368.
16. Goldberg, J. M., and Baldwin, R. L. (1998) Kinetic mechanism of a partial folding reaction. 1. Properties of the reaction and effects of denaturants. *Biochemistry 37*, 2546–2555.
17. Fersht, A. (1999) *Structure and mechanism in protein science* W. H. Freeman and Co., New York.
18. Bougie, I., Parent, A., and Bisaillon, M. (2004) Thermodynamics of ligand binding by the yeast mRNA-capping enzyme reveals different modes of binding. *Biochem. J. 384*, 411–420.
19. Ho, C. K., Schwer, B., and Shuman, S. (1998) Genetic, physical, and functional interactions between the triphosphatase and guanylyltransferase components of the yeast mRNA capping apparatus. *Mol. Cell. Biol. 18*, 5189–5198.
20. Ho, C. K., Lehman, K., and Shuman, S. (1999) An essential surface motif (WAQKW) of yeast RNA triphosphatase mediates formation of the mRNA capping enzyme complex with RNA guanylyltransferase. *Nucleic Acids Res. 27*, 4671–4678.
21. Fabrega, C., Shen, V., Shuman, S., and Lima, C. D. (2003) Structure of an mRNA Capping Enzyme Bound to the Phosphorylated Carboxy-Terminal Domain of RNA Polymerase II. *Mol. Cell 11*, 1549–1561.
22. McCracken, S., Fong, N., Rosonina, E., Yankulov, K., Brothers, G., Siderovski, D., Hessel, A., Foster, S., Amgen EST Program, Shuman, S., and Bentley, D. L. (1997) 5′-Capping enzymes are targeted to pre-mRNA by binding to the phosphorylated carboxy-terminal domain of RNA polymerase II. *Genes Dev. 11*, 3306–3318.
23. Lewis, J. D., and Izaurralde, E. (1997) The role of the cap structure in RNA processing and nuclear export. *Eur. J. Biochem. 247*, 461–169.
24. Nair, P. A., Nandakumar, J., Smith, P., Odell, M., Lima, C. D., and Shuman, S. (2007) Structural basis for nick recognition by a minimal pluripotent DNA ligase. *Nat. Struct. Mol. Biol. 14*, 770–778.

25. Fausnaugh, J., and Shatkin, A. J. (1990) Active site localization in a viral mRNA capping enzyme. *J. Biol. Chem. 265*, 7669–7672.
26. Reinisch, K. M., Nibert, M. L., and Harrison, S. C. (2000) Structure of the reovirus core at 3.6 Å resolution. *Nature 404*, 960–967.
27. Schwer, B., and Shuman, S. (1994) Mutational analysis of yeast mRNA capping enzyme. *Proc. Natl. Acad. Sci. U.S.A. 91*, 4328–4332.
28. Cong, P., and Shuman, S. (1995) Mutational analysis of mRNA capping enzyme identifies amino acids involved in GTP binding, enzyme-guanylate formation, and GMP transfer to RNA. *Mol. Cell. Biol. 91*, 6222–6231.
29. Sawaya, R., and Shuman, S. (2003) Mutational analysis of guanylyltransferase component of mammalian mRNA capping enzyme. *Biochemistry 42*, 8240–8249.
30. Ahola, T., and Kääriäinen, L. (1995) Reaction in alphavirus mRNA capping: Formation of a covalent complex of nonstructural protein nsP1 with 7-methyl-GMP. *Proc. Natl. Acad. Sci. U.S.A. 92*, 507–511.
31. Magden, J., Takeda, N., Li, T., Auvinen, P., Ahola, T., Miyamura, T., Merits, A., and Kaariainen, L. (2001) Virus-specific capping enzyme encoded by the hepatitis E virus. *J. Virol. 75*, 6249–6255.
32. Merits, A., Kettunen, R., Makinen, K., Lampio, A., Auvinen, P., Kaariainen, L., and Ahola, T. (1999) Virus-specific capping of tobacco mosaic virus RNA: Methylation of GTP prior to formation of covalent complex p126-^{m7}GMP. *FEBS Lett. 455*, 45–48.
33. Huang, Y. L., Hsu, Y. H., Han, Y. T., and Meng, M. (2005) mRNA guanylation catalyzed by the S-adenosylmethionine-dependent guanylyltransferase of bamboo mosaic virus. *J. Biol. Chem. 280*, 13153–13162.
34. Ahola, T., and Ahlquist, P. (1999) Putative RNA capping activities encoded by brome mosaic virus: Methylation and covalent binding of guanylate by replicase protein 1a. *J. Virol. 73*, 10061–10069.
35. Han, Y. X., Xue, R., Zhao, W., Zhou, Z. X., Li, J. N., Chen, H. S., Chen, X. H., Wang, Y. L., Li, Y. H., Wu, Y. W., You, X. F., Zhao, L. X., and Jiang, J. D. (2005) Antiviral therapeutic efficacy of foscarnet in hepatitis B virus infection. *Antiviral Res. 68*, 147–153.
36. Canestri, A., Ghosn, J., Wirden, M., Marguet, F., Ktorza, N., Boubezari, I., Dominguez, S., Bossi, P., Caumes, E., Calvez, V., and Katlama, C. (2006) Foscarnet salvage therapy for patients with late-stage HIV disease and multiple drug resistance. *Antiviral Ther. 11*, 561–566.
37. Derse, D., Bastow, K. F., and Cheng, Y. (1982) Characterization of the DNA polymerases induced by a group of herpes simplex type I variants selected for growth in the presence of phosphonoformic acid. *J. Biol. Chem. 257*, 10251–10260.

BI702054A